ACS APPLIED MATERIALS & INTERFACES

Research Article

www.acsami.org

$Li_4Ti_5O_{12}/TiO_2$ Hollow Spheres Composed Nanoflakes with Preferentially Exposed $Li_4Ti_5O_{12}$ (011) Facets for High-Rate Lithium Ion Batteries

Yan-Mei Jiang,[†] Kai-Xue Wang,*[,†] Xue-Yan Wu,[‡] Hao-Jie Zhang,[†] Bart M. Bartlett,[§] and Jie-Sheng Chen*[,†]

[†]School of Chemistry and Chemical Engineering, [‡]School of Materials Science and Engineering, Shanghai Jiao Tong University, Shanghai 200240, China

[§]Department of Chemistry, University of Michigan, 930 North University Avenue, Ann Arbor, Michigan 48109-1055, United States

Supporting Information

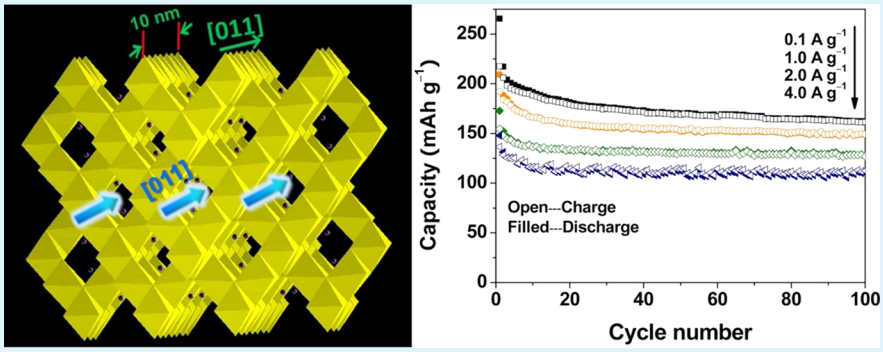

ABSTRACT: $Li_4Ti_5O_{12}/TiO_2$ hollow spheres composed of nanoflakes with preferentially exposed $Li_4Ti_5O_{12}$ (011) facets have been successfully fabricated via a facile hydrothermal processing route and following calcination. These hollow spheres show good electrochemical performance in terms of high capacity (266 mAh g^{-1} at 0.1 A g^{-1}), and excellent rate capability (110 mAh g^{-1} at 4.0 A g^{-1} up to 100 cycles), attributed to unique morphology, preferred facet orientation of the nanoflakes and microscopic structure of the hollow spheres. The preferentially exposed $Li_4Ti_5O_{12}$ (011) facets leads to fast lithium insertion/deinsertion processes in materials because of shorten lithium ion diffusion length, proved to be highly effective in improving the electrochemical properties of the hollow spheres. The excellent electrochemical performance makes these hollow spheres promising anode material for lithium ion batteries with high power and energy densities.

KEYWORDS: *$Li_4Ti_5O_{12}/TiO_2$ composite, nanoflakes, facet control, anode, lithium ion batteries*

1. INTRODUCTION

In past decades, titanium-oxide-based materials, particularly spinel $Li_4Ti_5O_{12}$ and anatase TiO_2, have been considered as promising anode materials for high power lithium ion batteries (LIBs) for electric vehicles and hybrid electric vehicles, due to their superior performance in terms of lithium ion intercalation/deintercalation and high safety.[1−6] Spinel $Li_4Ti_5O_{12}$ and anatase TiO_2 have many advantages over other anode materials. First, their respective frameworks provide abundant porous channels for fast lithium ion diffusion.[7−10] Second, the negligible volume change of spinel $Li_4Ti_5O_{12}$ and anatase TiO_2 electrodes during the insertion/extraction of lithium ions guarantees good cycling stability of the batteries.[2,11] Third, the high insertion voltage of spinel $Li_4Ti_5O_{12}$ and anatase TiO_2 can effectively avoid the formation of solid electrolyte interface (SEI) and lithium dendrites, ensuring good thermal stability and safety of the batteries.[1,2] These properties make spinel $Li_4Ti_5O_{12}$ and anatase TiO_2 alternatives to carbonaceous anodes for high performance lithium ion batteries.

However, the rate capability of titanium-oxide-based compounds is still quite low because of large polarization at high charge−discharge rates resulting from the poor electrical conductivity and sluggish lithium ion diffusion.[12−16] Many efforts have been focused on morphology tailoring and size control of the active materials to improve their electrochemical properties, and thus the rate capability.[17−22] Recently, the facet orientation of nanocrystalline particles has been shown to be critical in determining the performance of lithium battery electrodes.[23−31] Better reversibility and excellent rate capacity could be achieved for nanocrystalline TiO_2 polymorphs with dominant (001), (401), and (110) surfaces.[32−37] The mass

Received: July 30, 2014
Accepted: October 21, 2014
Published: October 21, 2014

transport property of spinel structures is strongly related to the exposed facets of crystalline particles, demonstrating that the facet exposure is an important factor that plays an essential role in determining the electrochemical performance of lithium battery electrodes.[38] Spinel $Li_4Ti_5O_{12}$ has plenty of porous channels along the [011] direction, favorable for fast lithium ion diffusion. Therefore, spinel $Li_4Ti_5O_{12}$ anodes with preferentially exposed (011) facets are highly desirable for high performance lithium ion batteries due to the directly accessible channels for the intercalation of lithium ions. In addition, the presence of binary or multiple components in one nanostructure is expected to store extra lithium ions within the interfacial area of the boundaries of these components, increasing the specific capacity of the nanostructure.[39−45]

Herein, we describe the preparation of $Li_4Ti_5O_{12}/TiO_2$ hollow spheres composed of nanoflakes with preferentially exposed $Li_4Ti_5O_{12}$ (011) facets through a simple hydrothermal process and subsequent calcination treatment. The $Li_4Ti_5O_{12}/TiO_2$ hollow spheres exhibit excellent electrochemical properties. The hierarchical hollow structure, the preferentially facet exposure of $Li_4Ti_5O_{12}$, and the presence of $Li_4Ti_5O_{12}/TiO_2$ dual phases are proved to be efficient in improving the electrochemical properties of electrode materials for lithium ion batteries.

2. EXPERIMENTAL SECTION

Preparation of Materials. The $Li_4Ti_5O_{12}/TiO_2$ hollow spheres were fabricated via hydrothermal and subsequent calcination processes by using porous amorphous TiO_2 prepared through a procedure reported previously[46] as a precursor. First, ethylene glycol and tetrabutyl titanate (1:10 by volume) were mixed at 160 °C for 2 h under vigorous stirring and then irradiated under ultraviolet (UV) light, generating the porous amorphous TiO_2 precursor. Then, 0.19 g of the amorphous TiO_2 precursor and 0.40 g of lithium hydroxide monohydrate were added to 40 mL of distilled water with continuous stirring. The obtained suspension was loaded into a 50 mL Teflon-lined stainless-steel autoclave and then heated at 130 °C for 7 d. The white product was collected by filtration, washed with ethanol thoroughly and dried naturally at room temperature, obtaining the hydrous lithium titanate precursor. The final $Li_4Ti_5O_{12}/TiO_2$ hollow spheres were generated by the calcination of the hydrous lithium titanate precursor at 400 °C for 2 h.

Characterization. X-ray diffraction (XRD) patterns were recorded on a Rigaku Dmax-2200 diffractometer (Rigaku, Japan) with Cu Kα radiation (λ = 1.5418 Å) at a scan rate of 6° min^{-1} within 5−70°. The morphology of the sample was observed with a scanning electron microscope (SEM, JSM-7401F, JEOL, Japan). JEM-2100F (JEOL, Japan) transmission electron microscope (TEM) operated at 200 kV. The specific surface areas of the samples were measured on a Micromeritics ASAP 2010 M+C nitrogen adsorption instrument (Micromeritices Inc., U.S.A.) at 77 K.

Electrochemical Measurements. Electrochemical properties of the $Li_4Ti_5O_{12}/TiO_2$ composite hollow spheres were evaluated with CR2016 coin cells. Active materials (obtained sample), acetylene black, and poly(vinylidene fluoride) (PVDF) binder were mixed at a weight ratio of 75:15:10 and dispersed in a *N*-methylpyrrolidone (NMP) solution to form a slurry. The slurry was coated on aluminum foil and dried in a vacuum oven at 110 °C overnight prior to coin-cell assembly. Lithium metal foil was used as both the counter and reference electrodes. A microporous polypropylene membrane (Celgard 2500) was used as the separator. The cells were assembled in an argon filled glovebox with both moisture and oxygen contents below 1.0 ppm. $LiClO_4$ of 1.0 M in ethylene carbonate/dimethyl carbonate (EC/DEC, 1:1 by volume) was employed as the electrolyte. The galvanostatic charge and discharge experiment was performed with a battery tester LAND-CT2001A in the voltage range 2.5−1.0 V at room temperature. The cyclic voltammetry (CV) curves were obtained on a Chenhua CHI 600B electrochemical station.

3. RESULTS AND DISCUSSION

The schematic illustration for the preparation of the $Li_4Ti_5O_{12}/TiO_2$ hollow spheres is shown in Scheme 1. Typically, titanium glycolate was first synthesized via heating the mixture of ethylene glycol and tetrabutyl titanate under vigorous stirring. The UV irradiation of the above titanium glycolate generates a porous amorphous titania. After hydrothermally treated with lithium hydroxide monohydrate in distilled water, the amorphous titania transforms into a hydrous lithium titanate precursor. Finally, the $Li_4Ti_5O_{12}/TiO_2$ hollow spheres were obtained through the calcination of the hydrous lithium titanate precursor.

Scheme 1. Schematic Illustration of the Preparation of $Li_4Ti_5O_{12}/TiO_2$ Hollow Spheres[a]

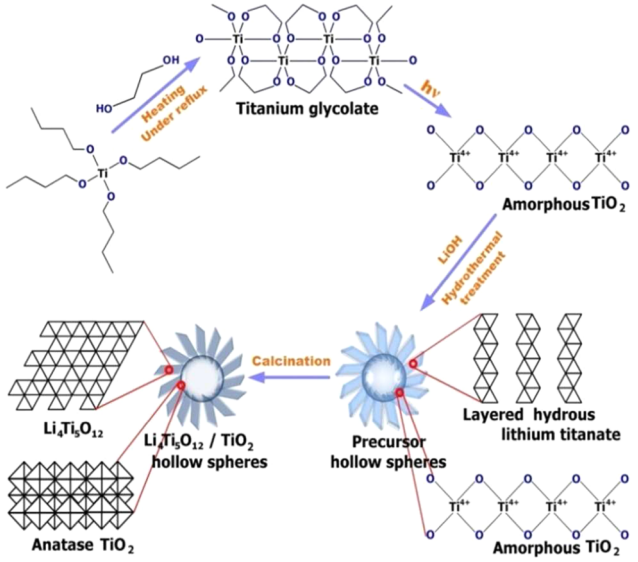

[a]The structures of anatase TiO_2, spinel $Li_4Ti_5O_{12}$, and layered hydrous lithium titanate represented by titanium oxygen octahedra, the Li^+ and H^+ lattice ions are not shown.

The XRD patterns of the precursor prepared hydrothermally and the $Li_4Ti_5O_{12}/TiO_2$ hollow spheres are shown in Figure S1 (Supporting Information) and Figure 1, respectively. All the diffraction peaks of the precursor (Figure S1) in the region of 2θ = 5−70° can be indexed in an orthorhombic cell of a layered hydrous lithium titanate with lattice constants of a = 16.66(2) Å, b = 3.797(2) Å, c = 3.007(3) Å (JCPDS No. 47−0123).[47] The peak at 2θ = 10.6° indicates the lamellar structure has a layer spacing of 0.84 nm (d_{200}). After calcinations at 400 °C for 2 h, the layered hydrous lithium titanate precursor transforms into spinel $Li_4Ti_5O_{12}$ (JCPDS No. 49-0207). As shown in Figure 1, the diffractions at 25.3°, 37.9°, 48.0°, 54.0°, and 55.2°, which can be assigned to anatase TiO_2 (JCPDS No. 21-1272) are also detected. The presence of the anatase TiO_2 might be resulted from the conversion of residual amorphous TiO_2 in the precursor. The content of spinel $Li_4Ti_5O_{12}$ in the composite is approximately 50 wt % based on the XRD analysis. The XRD analysis suggests that $Li_4Ti_5O_{12}/TiO_2$ composite is formed upon the calcination of the layered hydrous lithium titanate precursor.

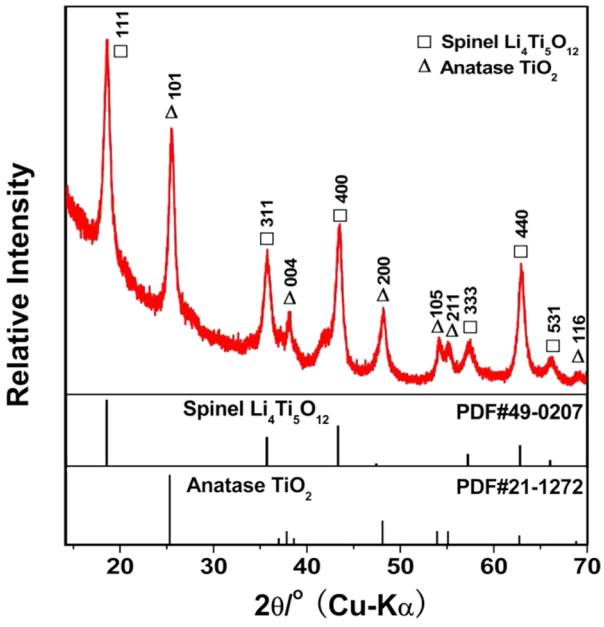

Figure 1. XRD pattern of the $Li_4Ti_5O_{12}/TiO_2$ composite hollow spheres.

The morphology and microstructure of the layered hydrous lithium titanate precursor was examined by SEM and TEM, as shown in Supporting Information Figure S2. The SEM images (Figure S2a) reveals a sphere-shaped morphology of the precursor assembled by nanoflakes. The diameter of the spheres is approximately 2 μm. These spheres are hollow inside as is shown by TEM (Figure S2b). The assembly of the nanoflakes forms the large interior void space and the well-defined shell. A typical single nanoflake has a length of approximately 1 μm and width of 200−400 nm (Figure S2c), and its single-crystalline nature is revealed by the selected area electron diffraction (SAED) pattern in Figure S2c (inset). In Figure S2d, the lattice fringes with d-spacing of 1.9 Å are ascribed to the (020) plane in orthorhombic structure. The high crystallinity and integrity of the nanoflake are also demonstrated by the Fast Fourier Transforms (FFT) of the image (inset in Figure S2d). The morphology evolution from amorphous titania to the layered hydrous lithium titanate hollow spheres is revealed by SEM observation of samples recovered during the hydrothermal preparation process (Figure S3). Based on SEM observation, the formation the hollow spheres might be due to the nucleation and cyrstal growth of hydrous lithium titanate on the surface of amorphous titania. The gradual consumption of amorpous titinia generates a hollow spheric structure.

The subsequent calcination to convert the layered hydrous lithium titanate leads to negligible change to the morphology of these hollow spheres (Figure 2a, Supporting Information Figure S4). As that of the layered hydrous lithium titanate, the hollow spheres of the calcined product are also composed of nanoflakes. The top view of the nanoflakes shown in the TEM image (Figure 2b) reveals the crystal structure of the nanoflakes. The lattice fringes with spacing of 0.49 nm are attributed to the (111) plane of spinel $Li_4Ti_5O_{12}$. The SAED pattern (inset in Figure 2b) taken along the [011] zone axis exhibits a series of spots pattern, indicating that the whole nanoflake has a "single-crystal-like" structure. All diffraction spots can be well indexed to a cubic $Li_4Ti_5O_{12}$ with lattice

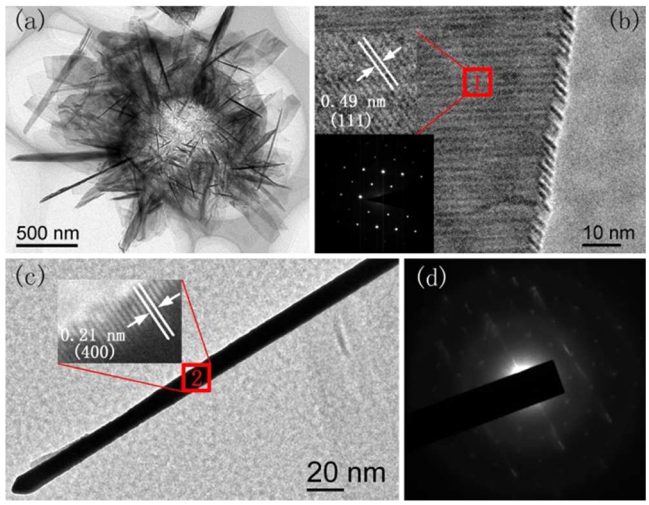

Figure 2. (a) TEM image of the $Li_4Ti_5O_{12}/TiO_2$ composite hollow spheres. (b,c) Different perspective high magnification TEM images of the same nanoflake. (b) TEM image of the nanoflake. The lower right inset in (b) shows the related SAED pattern from position 1, and the upper right inset is an enlarged TEM image. (c) TEM image of the nanoflake is recorded via the direction that parallel with the nanoflake plane observation. The inset in c is the corresponding HRTEM image. (d) NBED patterns corresponding to the marked zone 2 in c.

parameter of a = 8.358 Å. The side view of the nanoflake is shown in Figure 2c. The thickness of the nanoflakes is approximately 10 nm. The lattice fringes with a width of 0.21 nm in the corresponding HRTEM image are assigned to the (400) plane of spinel $Li_4Ti_5O_{12}$ (inset in Figure 2c). Figure 2d is nanobeam electron diffraction (NBED) pattern taken from position 2 in Figure 2c. This pattern is typical for a cubic structure, consistent with the SAED pattern in the inset of Figure 2b.

Figure 3 shows the top view HRTEM image of the nanoflake. It can be observed that two sets of lattices are present and that

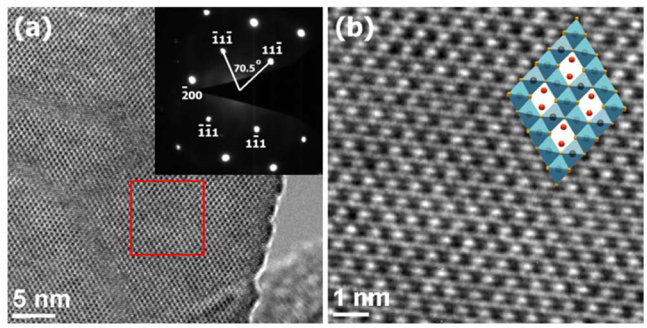

Figure 3. (a) HRTEM image of the surface of one side of the nanoflake (Inset: the corresponding SAED pattern). (b) Partial enlarged details of party of (a) red box. The inset in b shows the corresponding crystal structure of spinel $Li_4Ti_5O_{12}$ in projection along [011], expanded view of the framework built on TiO_6 or LiO_6 octahedra, with lithium ions in red.

they form a dihedral angel of approximately 70.5° to each other with an equal interfringe spacing of 0.49 nm, corresponding to the (111) planes of spinel $Li_4Ti_5O_{12}$. The corresponding SAED pattern of the same region (Figure 3a inset) can be indexed to diffraction spots of the [011] zone, indicating that nearly 100% of the exposed surfaces are (011) facets. The channels along the

[011] direction facilitate the fast penetration of lithium ions into the spinel $Li_4Ti_5O_{12}$ nanoflakes (Figure 3b inset). Moreover, the nanoflakes are only about 10 nm thick, significantly decreasing the diffusion distance of lithium ions along the favorable [011] direction. Nitrogen adsorption/desorption analyses indicate that the $Li_4Ti_5O_{12}/TiO_2$ composite has a BET specific surface area of approximately 97 $m^2\ g^{-1}$ and a pore volume of approximately 0.53 $cm^3\ g^{-1}$ (Supporting Information Figure S5). The mesopores have an average pore size of approximately 21 nm and their pore size distribution is quite broad.

The electrochemical performance of the $Li_4Ti_5O_{12}/TiO_2$ composite hollow spheres was evaluated in lithium half-cells. The cyclic voltammograms for the first two cycles shown in Figure 4 were conducted from 3.0 to 1.0 V (vs Li^+/Li) at a scan

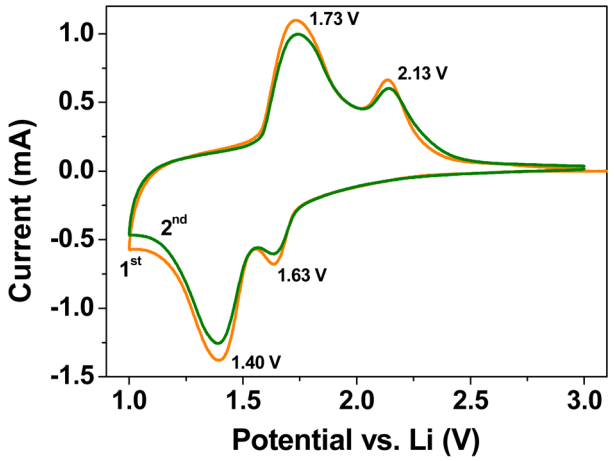

Figure 4. Cyclic voltammogram of the $Li_4Ti_5O_{12}/TiO_2$ composite hollow spheres between 3.0 and 1.0 V with a scan rate of 0.2 mV s^{-1}.

rate of 0.2 mV s^{-1}. In the first cycle, two pairs of cathodic/anodic peaks located at 1.40 V/1.73 V and 1.63 V/2.13 V are associated with lithium insertion/extraction within the spinel $Li_4Ti_5O_{12}$ and anatase TiO_2 lattices, respectively. In the following cycle, the peak potentials and curve shape remain virtually unchanged, suggesting the insertion/extraction of lithium-ion in the $Li_4Ti_5O_{12}/TiO_2$ composite hollow spheres is highly reversible. The capacity and cycle performance were evaluated by galvanostatic charge/discharge measurements at a current density of 0.1 A g^{-1} with a potential window ranging from 2.5 to 1.0 V (versus Li^+/Li) (Figure 5a).

In the discharge process, double potential plateaus due to different redox reactions associated with Li insertion are observed clearly. The first plateau at 1.75 V is ascribed to the phase transitions from anatase TiO_2 to orthorhombic phase Li_xTiO_2. The plateau at 1.55 V is attributed to the generation of rocksalt structure $Li_7Ti_5O_{12}$, resulting from the insertion of lithium ion into spinel $Li_4Ti_5O_{12}$. The long sloped region between 1.55 and 1.0 V is assigned to the pseudocapacitive lithium storage behavior of $Li_4Ti_5O_{12}$, which indicates the different electrochemical reaction characteristics including surface-confined charge-transfer or interfacial storage processes.[39−41,48,49] A high initial discharge/charge capacities of approximately 266 and 205 mAh g^{-1}, respectively, are achieved at a current density of 0.1 A g^{-1}, and they are closely related to the particular morphology of the $Li_4Ti_5O_{12}/TiO_2$ hollow spheres. As revealed by bright-field, dark-field TEM and HRTEM images, rich grain boundaries and defects are present

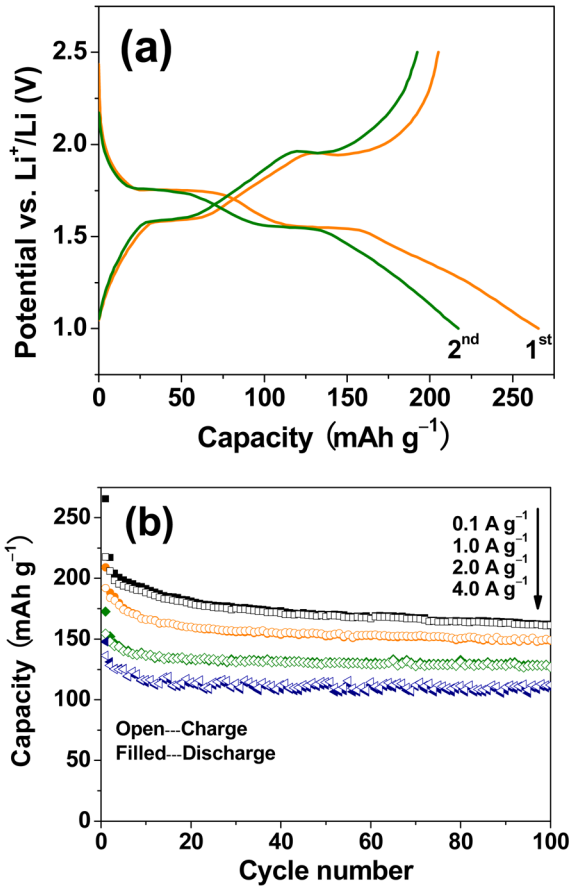

Figure 5. (a) Initial two discharge/charge curves of the $Li_4Ti_5O_{12}/TiO_2$ composite hollow sphere at 0.1 A g^{-1}. (b) Cycling performance of the $Li_4Ti_5O_{12}/TiO_2$ composite hollow sphere at 0.1, 1.0, 2.0, and 4.0 A g^{-1}, respectively.

in the nanoflakes of the material (Figure 3a and Supporting Information Figure S6). A large number of lithium ions can be stored on the interfacial area of the nanostructured material with high grain boundary densities, increasing the specific capacities of the material. The discharge/charge capacities of the second cycle are approximately 217 and 192 mAh g^{-1}, respectively, with the Coulombic efficiency significantly improved. The cycling performance of the $Li_4Ti_5O_{12}/TiO_2$ hollow spheres at the discharge/charge current densities of 0.1, 1.0, 2.0, and 4.0 A g^{-1} in the voltage range 2.5−1.0 V (versus Li^+/Li) is shown in Figure 5b. After cycling at 0.1 A g^{-1} for 100 cycles, the discharge capacity of the hollow spheres is approximately 162 mAh g^{-1}, indicating the good cycling stability. Cycled at a current density of 1.0, 2.0, and 4.0 A g^{-1}, the hollow spheres show a discharge capacity of 209, 173, and 148 mAh g^{-1} in the first cycle, and a high specific capacity of 149, 127, and 110 mAh g^{-1} after 100 cycles, giving a retention rate of approximately 71, 73, and 74%, respectively. The excellent electrochemical performance is mainly ascribed to the unique structural feature of the $Li_4Ti_5O_{12}/TiO_2$ hollow spheres built up by thin nanoflakes with preferentially exposed (011) facets. The kinetics of the lithium ion extraction/insertion process depends on lithium ion diffusion length in electrode materials. Compared with bulk materials, the nanoflakes, with a thickness of approximately 10 nm, significantly decreases the diffusion distance for lithium ions. The preferentially exposed (011) facets provide favorable lithium transport channels

(Figure 6), promoting the anisotropic diffusion of lithium ion within spinel $Li_4Ti_5O_{12}$ nanoflakes along the [011] zone channels upon charging and discharging.

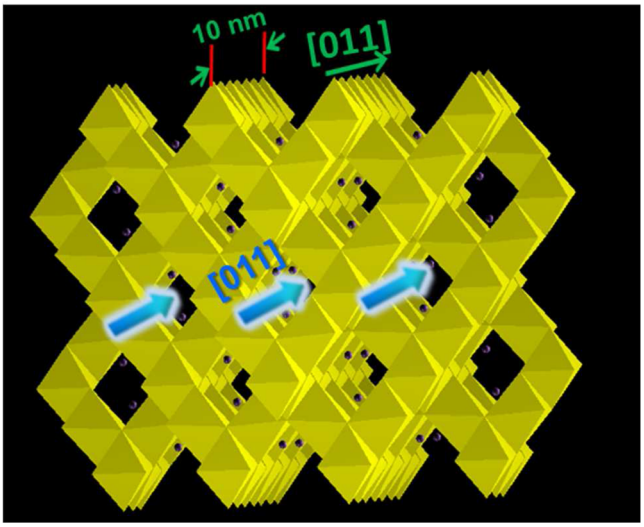

Figure 6. Schematic illustration of Li^+ diffusion in spinel structured $Li_4Ti_5O_{12}$, with Li ions in violet.

The superior electrochemical performance of the $Li_4Ti_5O_{12}/TiO_2$ hollow spheres constructed from nanoflakes is attributed to the synergistic effects of unique hierarchical morphology and microscopic structure. First, the hollow structure of the material facilitates the permeation of electrolyte within the electrode. The very thin nanoflakes that construct the hollow spheres significantly shorten the diffusion distance for lithium ions. The preferentially exposed (011) facets in the $Li_4Ti_5O_{12}$ nanoflakes provide directly accessible channels for the intercalation/deintercalation of lithium ions along the [011] direction. These structural features offer fast lithium insertion/extraction kinetics, leading to a high rate capability. Second, the existence of abundant grain boundaries in the dual-phase $Li_4Ti_5O_{12}/TiO_2$ composite can store extra lithium ions than single phase spinel $Li_4Ti_5O_{12}$ or anatase TiO_2, ensuring the high specific capacity of the composite. In addition, the hollow structure and thin nanoflakes also accommodate the possible stress induced during the discharge/charge process effectively, which results in good structural and cycling stability.

4. CONCLUSIONS

$Li_4Ti_5O_{12}/TiO_2$ hollow spheres composed of nanoflakes with nearly 100% exposed $Li_4Ti_5O_{12}$ (011) facets have been successfully fabricated by a template-free hydrothermal route. The obtained $Li_4Ti_5O_{12}/TiO_2$ hollow spheres exhibit excellent electrochemical performance. A high initial discharge capacity of 266 mAh g^{-1} is delivered at 0.1 A g^{-1} and a capacity of 110 mAh g^{-1} is still retained upon cycling at a high rate of 4.0 A g^{-1} for 100 cycles. The combination of the unique hollow sphere morphology, preferred facet orientation of nanoflakes, and grain boundaries among the $Li_4Ti_5O_{12}$ and TiO_2 components contributes to the large specific discharge and charge capacities, high rate capability, and good cycling stability of the $Li_4Ti_5O_{12}/TiO_2$ hollow spheres. These merits make $Li_4Ti_5O_{12}/TiO_2$ material a promising candidate as an anode material for high performance lithium ion batteries.

■ ASSOCIATED CONTENT

Supporting Information

Characterization of the layered hydrous lithium titanate precursor and $Li_4Ti_5O_{12}/TiO_2$ hollow spheres, XRD patterns and SEM, TEM of the layered hydrous lithium titanate precursor and $Li_4Ti_5O_{12}/TiO_2$ hollow spheres, SEM images of the precipitates obtained at different reaction time during the hydrothermal preparation process, BET of the $Li_4Ti_5O_{12}/TiO_2$ hollow spheres. This material is available free of charge via the Internet at http://pubs.acs.org.

■ AUTHOR INFORMATION

Corresponding Authors

*E-mail: k.wang@sjtu.edu.cn.
*E-mail: chemcj@sjtu.edu.cn.

Notes

The authors declare no competing financial interest.

■ ACKNOWLEDGMENTS

This work was financially supported by the National Basic Research Program (2014CB932102, 2013CB934102) and the National Natural Science Foundation of China (21271128, 21331004, 21301117). K.X.W. and B.M.B. are also grateful for the support from a SJTU-UM Collaborative Research Project.

■ REFERENCES

(1) Ohzuku, T.; Ueda, A.; Yamamota, N. Zero-Strain Insertion Material of $Li[Li_{1/3}Ti_{5/3}]]O_4$ for Rechargeable Lithium Cells. *J. Electrochem. Soc.* **1995**, *142*, 1431−1435.
(2) Wagemaker, M.; Kearley, G. J.; Well, A. A. v.; Mutka, H.; Mulder, F. M. Multiple Li Positions inside Oxygen Octahedra in Lithiated TiO_2 Anatase. *J. Am. Chem. Soc.* **2003**, *125*, 840−848.
(3) Ohzuku, T.; Takehara, Z.; Yoshizawa, S. Nonaqueous Lithium/Titanium Dioxide Cell. *Electrochim. Acta* **1979**, *24*, 219−222.
(4) Armstrong, A. R.; Armstrong, G.; Canales, J.; Bruce, P. G. TiO_2-B Nanowires. *Angew. Chem., Int. Ed.* **2004**, *43*, 2286−2288.
(5) Reddy, M. A.; Kishore, M. S.; Pralong, V.; Varadaraju, U. V.; Raveau, B. Lithium Intercalation into Nanocrystalline Brookite TiO_2. *Electrochem. Solid-State Lett.* **2007**, *10*, A29−A31.
(6) Ohzuku, T.; Sawai, K.; Hira, T. Topotactic Two-Phase Reaction of Ruthenium Dioxide (Rutile) in Lithium Nonaqueous Cell. *J. Electrochem. Soc.* **1990**, *139*, 3004−3010.
(7) Wang, G. X.; Bradhurst, D. H.; Dou, S. X.; Liu, H. K. Spinel $Li[Li_{1/3}Ti_{5/3}]O_4$ as an Anode Material for Lithium Ion Batteries. *J. Power Sources* **1999**, *83*, 156−161.
(8) Zhang, Y.; Zheng, H.; Liu, G.; Battaglia, V. Synthesis and Electrochemical Studies of a Layered Spheric TiO_2 through Low Temperature Solvothermal Method. *Electrochim. Acta* **2009**, *54*, 4079−4083.
(9) Kanamura, K.; Naito, H.; Takehara, Z. Novel Spinel Oxide $Li_{4/3}Ti_{5/3}O_4$ as Electrochemical Insertion Materials for Rechargeable Lithium Batteries. *Chem. Lett.* **1997**, *26*, 45−46.
(10) Ge, H.; Li, N.; Li, D.; Dai, C.; Wang, D. Study on the Theoretical Capacity of Spinel Lithium Titanate Induced by Low-Potential Intercalation. *J. Phys. Chem. C* **2009**, *113*, 6324−6326.
(11) Scharner, S.; Weppner, W.; Schmid-Beurmannb, P. Evidence of Two-Phase Formation upon Lithium Insertion into the $Li_{1.33}Ti_{1.67}O_4$ Spinel. *J. Electrochem. Soc.* **1999**, *146* (3), 857−861.
(12) Cheng, L.; Li, X. L.; Liu, H. J.; Xiong, H. M.; Zhang, P. W.; Xia, Y. Y. Carbon-Coated $Li_4Ti_5O_{12}$ as a High Rate Electrode Material for Li-Ion Intercalation. *J. Electrochem. Soc.* **2007**, *154*, A692−A697.
(13) Liu, H.; Feng, Y.; Wang, K.; Xie, J. Y. Synthesis and Electrochemical Properties of $Li_4Ti_5O_{12}/C$ Composite by the PVB Rheological Phase Method. *J. Phys. Chem. Solids* **2008**, *69*, 2037−2040.
(14) Cheng, L.; Yan, J.; Zhu, G. N.; Luo, J. Y.; Wang, C. X.; Xia, Y. Y. General Synthesis of Carbon-Coated Nanostructure $Li_4Ti_5O_{12}$ as a

High Rate Electrode Material for Li-Ion Intercalation. *J. Mater. Chem.* **2010**, *20*, 595−602.
(15) Wang, J.; Liu, X. M.; Yang, H.; Shen, X. d. Characterization and Electrochemical Properties of Carbon-Coated $Li_4Ti_5O_{12}$ Prepared by a Citric Acid Sol−Gel Method. *J. Alloys Compd.* **2011**, *509*, 712−718.
(16) Zhu, G. N.; Wang, C. X.; Xia, Y. Y. A Comprehensive Study of Effects of Carbon Coating on $Li_4Ti_5O_{12}$ Anode Material for Lithium-Ion Batteries. *J. Electrochem. Soc.* **2011**, *158*, A102−A109.
(17) Kubiak, P.; Fröschl, T.; Hüsing, N.; Hörmann, U.; Kaiser, U.; Schiller, R.; Weiss, C. K.; Landfester, K.; Wohlfahrt-Mehrens, M. TiO_2 Anatase Nanoparticle Networks: Synthesis, Structure, and Electrochemical Performance. *Small* **2011**, *7*, 1690−1696.
(18) Liu, S.; Jia, H.; Han, L.; Wang, J.; Gao, P.; Xu, D.; Yang, J.; Che, S. Nanosheet-Constructed Porous TiO_2−B for Advanced Lithium Ion Batteries. *Adv. Mater.* **2012**, *24*, 3201−3204.
(19) Jiang, Y. M.; Wang, K. X.; Guo, X. X.; Wei, X.; Wang, J. F.; Chen, J. S. Mesoporous Titania Rods as an Anode Material for High Performance Lithium-Ion Batteries. *J. Power Sources* **2012**, *214*, 298−302.
(20) Chen, J.; Yang, L.; Fang, S.; Tang, Y. Synthesis of Sawtooth-like $Li_4Ti_5O_{12}$ Nanosheets as Anode Materials for Li-Ion Batteries. *Electrochim. Acta* **2010**, *55*, 6596−6600.
(21) Tang, Y. F.; Yang, L.; Fang, S. H.; Qiu, Z. $Li_4Ti_5O_{12}$ HolLow Microspheres Assembled by Nanosheets as an Anode Material for High-Rate Lithium Ion Batteries. *Electrochim. Acta* **2009**, *54*, 6244−6249.
(22) Hao, X.; Bartlett, B. M. $Li_4Ti_5O_{12}$ Nanocrystals Synthesized by Carbon Templating from Solution Precursors Yield High Performance Thin Film Li-Ion Battery Electrodes. *Adv. Energy Mater.* **2013**, *3*, 753−761.
(23) Jung, S. C.; Han, Y. K. Facet-Dependent Lithium Intercalation into Si Crystals: Si(100) vs Si(111). *Phys. Chem. Chem. Phys.* **2011**, *13*, 21282−21287.
(24) Liang, L.; Zhou, M.; Xie, Y. Electrospun Hierarchical LiV_3O_8 Nanofibers Assembled from Nanosheets with Exposed {100} Facets and Their Enhanced Performance in Aqueous Lithium-Ion Batteries. *Chem.—Asian J.* **2012**, *7*, 565−571.
(25) Yang, S.; Zhou, X.; Zhang, J.; Liu, Z. Morphology-Controlled Solvothermal Synthesis of $LiFePO_4$ as a Cathode Material for Lithium-Ion Batteries. *J. Mater. Chem.* **2010**, *20*, 8086−8091.
(26) Nan, C.; Lu, J.; Chen, C.; Peng, Q.; Li, Y. Solvothermal Synthesis of Lithium Iron Phosphate Nanoplates. *J. Mater. Chem.* **2011**, *21*, 9994−9996.
(27) Guan, X. F.; Zheng, J.; Zhao, M. L.; Li, L. P.; Li, G. S. Synthesis of $FeTiO_3$ Nanosheets with {0001} Facets Exposed: Enhanced Electrochemical Performance and Catalytic Activity. *RSC Adv.* **2013**, *3*, 13635−13641.
(28) Qin, X.; Wang, J.; Xie, J.; Li, F.; Wen, L.; Wang, X. Hydrothermally Synthesized $LiFePO_4$ Crystals with Enhanced Electrochemical Properties: Simultaneous Suppression of Crystal Growth along [010] and Antisite Defect Formation. *Phys. Chem. Chem. Phys.* **2012**, *14*, 2669−2677.
(29) Fu, F.; Xu, G. L.; Wang, Q.; Deng, Y. P.; Li, X.; Li, J. T.; Huang, L.; Sun, S. G. Synthesis of Single Crystalline Hexagonal Nanobricks of $LiNi_{1/3}Co_{1/3}Mn_{1/3}O_2$ with High Percentage of Exposed {010} Active Facets as High Rate Performance Cathode Material for Lithium-Ion Battery. *J. Mater. Chem. A* **2013**, *1*, 3860−3864.
(30) Sun, W.; Cao, F.; Liu, Y.; Zhao, X.; Liu, X.; Yuan, J. Nanoporous $LiMn_2O_4$ Nanosheets with Exposed {111} Facets as Cathodes for Highly Reversible Lithium-Ion Batteries. *J. Mater. Chem.* **2012**, *22*, 20952−20957.
(31) Hirayama, M.; Ido, H.; Kim, K.; Cho, W.; Tamura, K.; Mizuki, J.; Kanno, R. Dynamic Structural Changes at $LiMn_2O_4$/Electrolyte Interface during Lithium Battery Reaction. *J. Am. Chem. Soc.* **2010**, *132*, 15268−15276.
(32) Chen, J. S.; Lou, X. W. Unusual Rutile TiO_2 Nanosheets with Exposed (001) Facets. *Chem. Sci.* **2011**, *2*, 2219−2223.
(33) Ding, S.; Chen, J. S.; Wang, Z.; Cheah, Y. L.; Madhavi, S.; Hu, X.; Lou, X. W. TiO_2 Hollow Spheres with Large Amount of Exposed (001) Facets for Fast Reversible Lithium Storage. *J. Mater. Chem.* **2011**, *21*, 1677−1680.
(34) Etacheri, V.; Kuo, Y.; Van der Ven, A.; Bartlett, B. M. Mesoporous TiO_2-B Microflowers Composed of $(1\bar{1}0)$ Facet-Exposed Nanosheets for Fast Reversible Lithium-ion Storage. *J. Mater. Chem. A* **2013**, *1*, 12028−12032.
(35) Han, X.; Zhou, F.; Li, L.; Wang, C. Morphology Control of Anatase TiO_2 Spindly Octahedra with Exposed High-Index {401} Facets and Application in Lithium-Ion Batteries. *Chem.—Asian J.* **2013**, *8*, 1399−1403.
(36) Wang, Z.; Zhang, Y.; Xia, T.; Murowchick, J.; Liu, G.; Chen, X. Lithium-Ion Battery Performance of (001)-Faceted TiO_2 Nanosheets vs Spherical TiO_2 Nanoparticles. *Energy Technol.* **2014**, *2*, 376−382.
(37) Sun, C. H.; Yang, X. H.; Chen, J. S.; Li, Z.; Lou, X. W.; Li, C.; Smith, S. C.; Lu, G. Q.; Yang, H. G. Higher Charge/Discharge Rates of Lithium-ions across Engineered TiO_2 Surfaces Leads to Enhanced Battery Performance. *Chem. Commun.* **2010**, *46*, 6129−6131.
(38) Hai, B.; Shukla, A. K.; Duncan, H.; Chen, G. The Effect of Particle Surface Facets on the Kinetic Properties of $LiMn_{1.5}Ni_{0.5}O_4$ Cathode Materials. *J. Mater. Chem. A* **2013**, *1*, 759−769.
(39) Guo, X.; Fang, X.; Mao, Y.; Wang, Z.; Wu, F.; Chen, L. Capacitive Energy Storage on Fe/Li_3PO_4 Grain Boundaries. *J. Phys. Chem. C* **2011**, *115*, 3803−3808.
(40) Yu, X. Q.; Sun, J. P.; Tang, K.; Li, H.; Huang, X. J.; Dupont, L.; Maier, J. Reversible Lithium Storage in LiF/Ti Nanocomposites. *Phys. Chem. Chem. Phys.* **2009**, *11*, 9497−9503.
(41) Li, X.; Lai, C.; Xiao, C. W.; Gao, X. P. Enhanced High Rate Capability of Dual-Phase $Li_4Ti_5O_{12}$-TiO_2 Induced by Pseudocapacitive Effect. *Electrochim. Acta* **2011**, *56*, 9152−9158.
(42) Rahman, M. M.; Wang, J. Z.; Hassan, M. F.; Chou, S. L.; Wexler, D.; Liu, H. K. Basic Molten Salt Process a New Route for Synthesis of Nanocrystalline $Li_4Ti_5O_{12}$-TiO_2 Anode Material for Li-Ion Batteries Using Eutectic Mixture of $LiNO_3$-LiOH-Li_2O_2. *J. Power Sources* **2010**, *195*, 4297−4303.
(43) Rahman, M. M.; Wang, J. Z.; Hassan, M. F.; Wexler, D.; Liu, H. K. Amorphous Carbon Coated High Grain Boundary Density Dual Phase $Li_4Ti_5O_{12}$-TiO_2: A Nanocomposite Anode Material for Li-Ion Batteries. *Adv. Energy Mater.* **2011**, *1*, 212−220.
(44) Wang, Y. Q.; Gu, L.; Guo, Y. G.; Li, H.; He, X. Q.; Tsukimoto, S.; Ikuhara, Y.; Wan, L. Rutile-TiO_2 Nanocoating for a High-Rate $Li_4Ti_5O_{12}$ Anode of a Lithium-Ion Battery. *J. Am. Chem. Soc.* **2012**, *134*, 7874−7879.
(45) Jiang, Y. M.; Wang, K. X.; Zhang, H. J.; Wang, J. F.; Chen, J. S. Hierarchical $Li_4Ti_5O_{12}$/TiO_2 Composite Tubes with Regular Structural Imperfection for Lithium Ion Storage. *Sci. Rep.* **2013**, *3*, 3490.
(46) Zou, X. X.; Li, G. D.; Wang, K. X.; Li, L.; Su, J.; Chen, J. S. Light-induced Formation of Porous TiO_2 with Superior Electron-Storing Capacity. *Chem. Commun.* **2010**, *46*, 2112−2114.
(47) Sugita, M.; Tsuji, M.; Abe, M. Synthetic Inorganic Ion-Exchange Materials. LVIII. Hydrothermal Synthesis of a New Layered Lithium Titanate and Its Alkali Ion Exchange. *Bull. Chem. Soc. Jpn.* **1990**, *63*, 1978−1984.
(48) Jamnik, J.; Maier, J. Nanocrystallinity Effects in Lithium Battery Materials Aspects of Nano-Ionics. Part IV. *Phys. Chem. Chem. Phys.* **2003**, *5*, 5215−5220.
(49) Lai, C.; Dou, Y. Y.; Li, X.; Gao, X. P. Improvement of the High Rate Capability of Hierarchical Structured $Li_4Ti_5O_{12}$ Induced by the Pseudocapacitive Effect. *J. Power Sources* **2010**, *195*, 3676−3679.